Design and Realization of a Novel Optically Disordered Material: A Demonstration of a Mie Glass

José M. Miranda-Muñoz, Gabriel Lozano, and Hernán Míguez**

Herein, a diffusive material presenting optical disorder is introduced, which represents an example of a Mie glass. Comprising spherical crystalline TiO_2 nanoparticles randomly dispersed in a mesoporous TiO_2 matrix, it is proved that the scattering of light in this inhomogeneous solid can be predicted in an unprecedented manner from single-particle considerations employing Mie theory. To that aim, a study of the dependence of the key parameters employed is performed to describe light propagation in random media, i.e., the scattering mean free path and the transport mean free path, as a function of the size and concentration of the spherical inclusions based on a comparison between experimental results and analytical calculations. It is also demonstrated that Mie glasses enable enhanced fluorescence intensity due to a combined absorptance enhancement of the excitation light combined with an improved outcoupling of the emitted light. The method offers the possibility to perform a deterministic design for the realization of a light diffuser with tailor-made scattering properties.

1. Introduction

It is well known that the optical properties of dilute dispersions of spherical particles in liquid media can be understood based on the analytical results of Mie theory.[1,2] As long as the concentration of scatterers allows neglecting correlation effects, the behavior of the system can be easily extrapolated from that of the individual particles. Simultaneously, liquid media offer several advantages. First, they typically present a low refractive index, which favors reaching a high dielectric contrast between the medium and the dispersed phase, reinforcing the scattering strength of the scatterers.[3–9] In addition, they can serve as solvents of chromophores of different sort, whose absorption, and therefore emission intensity, can be enhanced by means of multiple scattering occurring in the dispersion. Such features were taken advantage of in the 90's of the 20th century to develop random lasers.[10]

When it comes to solids, most attempts to realize multiple scattering media have been based on packings of high refractive index particles of variable dispersity to demonstrate novel transport properties with applications in optoelectronic devices such as solar cells,[11–13] random lasers,[14–16] or white light-emitting diodes.[17,18] The actual spectral response of these systems, except for the case of photonic glasses, i.e., disordered packings attained from quasi-monodisperse colloids,[19–22] cannot be predesigned on the basis of analytical models. However, significant efforts have been devoted lately to develop strategies to select the scattering properties of diffusive materials prior to fabrication.[23]

Herein, we introduce an optically random solid slab that behaves similarly to a liquid dispersion of monodisperse particles. Not only its optical response can be predetermined based on Mie theory, but also allows for a large amount of chromophores to be loaded, as it is based on a high specific surface area (≈150 m^2 cm^{-3}) matrix embedding strongly scattering particles. A synthetic route to maximize the refractive index contrast between the two phases present in the material is also demonstrated. A full optical characterization is performed to attain all relevant parameters, namely, scattering (l_{sc}) and transport mean free paths (l_t), which are in fair agreement with Mie theory. The potential of this material that represents a novel demonstration of a Mie glass is confirmed by soaking the films in fluorescent dyes, whose spontaneous emission is enhanced by a factor of approximately three due to the combined effect of absorption reinforcement and outcoupling improvement.

2. Modeling

We performed an analytical study of our Mie glass based on Mie theory prior to material realization. A series of different available materials that can be synthesized in the form of a colloid of spherical particles, such as silicon oxide (SiO_2), titanium oxide (TiO_2), or polystyrene spheres, were considered. Based on a practical criterion, possible mesoporous matrices where to embed those particles were modeled. These included low density media for which a wide number of synthetic methods had been developed, such as mesostructured SiO_2 and TiO_2. Also, the effect of void scatterers, which would result from the etching of organic spheres in an inorganic matrix, was also accounted for. We assessed light propagation in Mie glasses based on the standard parameters used to characterized optically random media, i.e., l_{sc} and l_t. In particular, the model

J. M. Miranda-Muñoz, Dr. G. Lozano, Prof. H. Míguez
Multifunctional Optical Materials Group
Institute of Materials Science of Sevilla
Consejo Superior de Investigaciones
Científicas – Universidad de Sevilla (CSIC-US)
Américo Vespucio 49, 41092 Sevilla, Spain
E-mail: g.lozano@csic.es; h.miguez@csic.es

DOI: 10.1002/adom.201700025

assumes that the average distance at which a photon propagating through a solid dispersion of spherical scatterers within a porous matrix undergoes a scattering event is given by

$$l_{sc} = \frac{\frac{4}{3}\pi r^3}{f \cdot \sigma_{sc}} \quad (1)$$

where f is the particle volume filling fraction, r is the radius of the scatterers, and σ_{sc} is the scattering cross-section, which is determined by the complex refractive index of both the scattering particle (N_p) and the medium (N_m), as well as by the particle size and shape through the expression derived by Mie

$$\sigma_{sc} = \frac{2\pi}{k^2}\sum_{n=1}^{\infty}(2n+1)\left(|a_n|^2 + |b_n|^2\right) \quad (2)$$

where $k = \frac{2\pi}{\lambda n_m}$ is the modulus of the wave vector with λ being the wavelength of light and n_m the real part of N_m.[1] For a generic spherical scatterer, the coefficients a_n and b_n of Equation (2) can be written as a function of the Riccati–Bessel functions as it is described in the Supporting Information. l_t is the length over which the direction of propagation of the photon is randomized, and it depends on the angular distribution of the scattering through the following expression[24]

$$l_t = \frac{l_{sc}}{1 - \langle \cos\theta \rangle} \quad (3)$$

where θ is the scattering angle measured from the direction of the illumination, and the average of $\cos\theta$ is calculated weighting the contribution of each θ according to the angular distribution of scattered intensity provided by Mie theory. A small sphere, in relation to the wavelength of the incident light, presents a dipole-like scattering. For larger spheres, however, the scattering becomes mainly forward. We have demonstrated elsewhere that spherical scatterers yield the most efficient scattering of light in the forward direction when compared to large particles of similar size but other shape.[25] Moreover, the symmetry of the sphere ensures that light is scattered the same way regardless the incident direction of incoming light. As it was our goal to find optically random media that could serve to enhance the emission of dyes at optical frequencies, we focused on systems that, combining the materials available, displayed the shortest l_{sc} at visible wavelengths. Among those candidates that perform the best as a multiple scattering system, we chose that made of titanium dioxide (TiO_2) spheres surrounded by a thin void layer and embedded in a porous TiO_2 matrix. This is practically achievable by playing with the different contraction of scatterers and the matrix when subjected to thermal treatments.[25] Theoretical predictions for other optically random materials, as well as their experimental realizations, can be consulted in the Supporting Information.

Figure 1a shows the spectral distribution of σ_{sc} of a TiO_2 sphere embedded in a TiO_2 mesoporous matrix as a function of the sphere size. Calculations displayed in Figure 1a indicate that the scattering strength increases with the radius of the sphere for each wavelength, showing a resonant response for

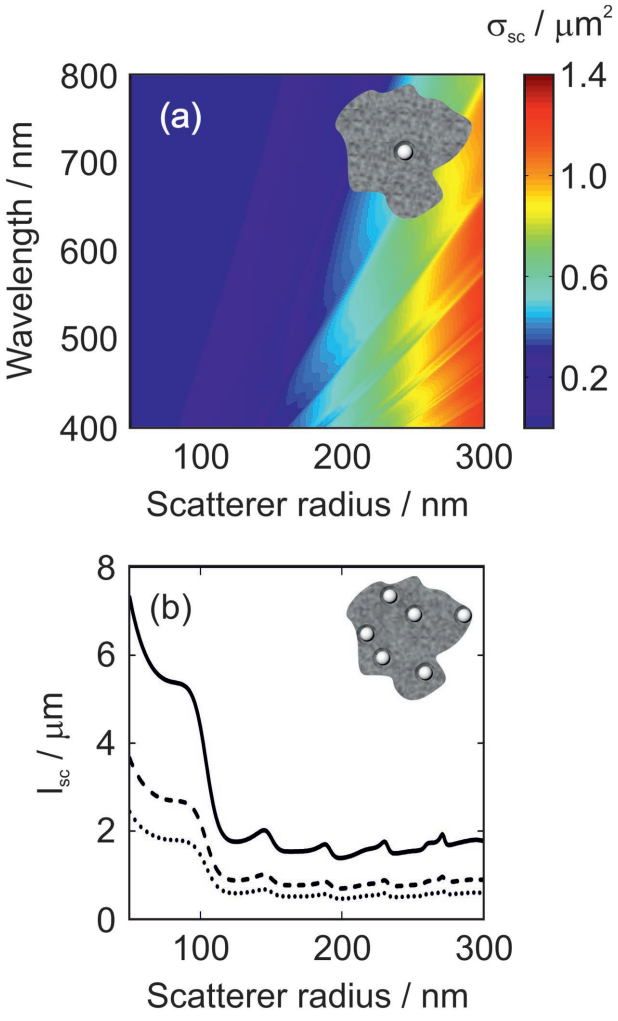

Figure 1. a) Calculation of the wavelength-dependent scattering cross-sections for crystalline TiO_2 nanospheres of different radius embedded in a mesoporous TiO_2 matrix. b) Calculated scattering mean free path at λ = 530 nm versus the radius of the scattering centers for films with filling fraction f = 5% (solid line), f = 10% (dashed line), and f = 15% (dotted line).

specific values of r, as it is well known.[24,26] Similar behavior has been observed in other resonant nanostructures.[27] Figure 1b shows the dependence of l_{sc} with the sphere radius for three values of the volume filling fraction: f = 5%, f = 10%, and f = 15% at λ = 530 nm. For larger volume fractions the model should include more advanced contributions from dependent scattering and structure factor.[28] Overall, it can be observed that for a given wavelength and a given size of the scatterer the l_{sc} reduces with increasing f, which implies longer residence times of the light in the material, due to a larger scattering strength of the system. According to our calculations, the porosity of the embedding medium plays an important role, as further discussed in the Supporting Information. We will exclusively focus on matrices presenting 50% porosity, which is actually one of the most efficient matrices for the type of scatterer (dense titania surrounded by an air corona) herein considered.

3. Experimental Realization

In view of the calculations, we choose spheres of two sizes, namely, $r = 225$ nm and $r = 95$ nm and three different particle density: $f = 5\%$, $f = 10\%$, and $f = 15\%$, so as to demonstrate scattering media with distinct scattering properties. For the experimental realization of our Mie glass, crystalline submicron TiO_2 spheres of similar sizes were dispersed in a random manner in a mesoporous TiO_2 matrix as it is shown in the scanning electron microscope (SEM) images of **Figure 2**a,b. Layers with thicknesses ranging from ~2 µm to ~12 µm were prepared by means of solution processing in a one-deposition step, with no need of further treatments other than the thermal annealing required to achieve mechanical stability, following the procedure described in detail in the Experimental Section.

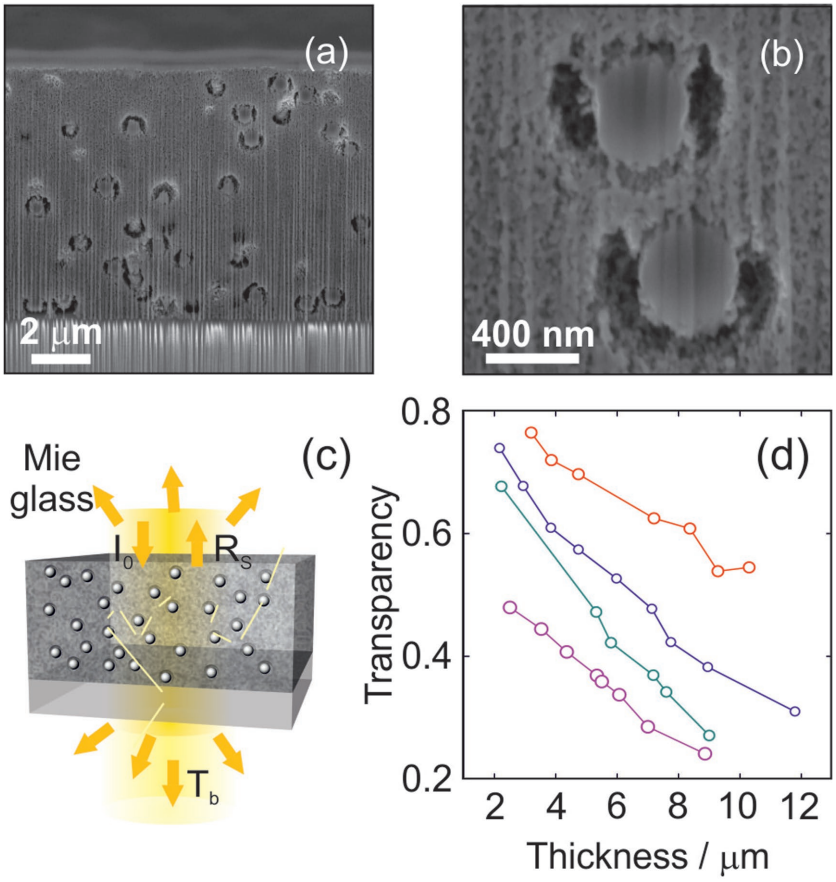

Figure 2. a) Dual column focused ion beam–secondary electron microscopy image of a cross-section of a 7.5 µm thick film made of TiO_2 spherical inclusions of radius $r = 225 \pm 20$ nm surrounded by an air shell embedded in a mesoporous TiO_2 matrix with filling fraction of $f = 5\%$. b) Zoom-in of the mesoporous matrix in which the spherical shape of the scatterers is observed. c) Schematic of a Mie glass. d) Transparency as a function of film thickness for different Mie glasses made of TiO_2 spheres of radius r embedded in a TiO_2 porous matrix at a filling fraction f, namely, $r = 95 \pm 20$ nm and $f = 5\%$ (red symbols); $r = 225 \pm 20$ nm and $f = 5\%$ (blue symbols); $r = 225 \pm 20$ nm and $f = 10\%$ (green symbols); and $r = 225 \pm 20$ nm and $f = 15\%$ (magenta symbols). Colored lines are only guides to the eye.

4. Optical Characterization

A spectroscopic analysis of the light reflected and transmitted by Mie glasses—as schemed in Figure 2c—is performed in order to assess their performance as light diffusers (see the Supporting Information for the complete set of experimental data). Figure 2d displays the transparency of the scattering media, defined as $\int_{400}^{2000} T_b(\lambda)\mathrm{d}\lambda$ where T_b is the ballistic transmittance, as a function of their thickness. Notice that a transparency value of 1 corresponds to a medium through which light goes through without being scattered. Results displayed in Figure 2d show that (i) transparency decreases with film thickness, (ii) the material becomes more diffusive for bigger scattering centers due to the fact that larger spheres feature higher scattering cross-sections (see Figure 1a), and (iii) if the size of the spheres remains fixed, larger values of f yield shorter l_{sc} (see Figure 1b), and therefore highly diffusive media.

4.1. Analysis of the Scattering Parameters

The spectral l_{sc} can be determined from experimental measurements employing a model based on the Lambert–Beer law, according to

$$\frac{T_b}{1-R_s} = e^{-L/l_{sc}} \tag{4}$$

with R_s being the specular reflectance of the system and L the thickness of the layer. The complete derivation of Equation (2) can be found in the Supporting Information. To illustrate this, **Figure 3**a features the thickness dependence of $\ln\left(\frac{T_b}{1-R_s}\right)$ at $\lambda = 800$ nm for the Mie glasses analyzed in Figure 2, which shows a linear dependence. From the comparison of the different curves in Figure 3a, it is clear that the slope of the linear fitting increases when larger scattering centers or higher loading fractions are considered. Higher slopes imply shorter values of l_{sc} as displayed in Figure 3b. Figure 3c shows the calculated l_{sc} according to Equation (1). A fair agreement is found between experimental and calculated l_{sc}, revealing that it is possible to describe the scattering behavior of these optically disordered films qualitatively and, to a good extent, quantitatively from analytical calculations based on single-sphere considerations, hence confirming their behavior as Mie glasses. Please notice that l_{sc} values are extracted from linear fittings in which $r^2 > 0.95$. For the wavelengths at which this condition is not fulfilled, it is thus not possible to extract a faithful value of l_{sc} from the measurements. The reason for this deviation may reside in the fact that, for longer wavelengths, l_{sc} is expected

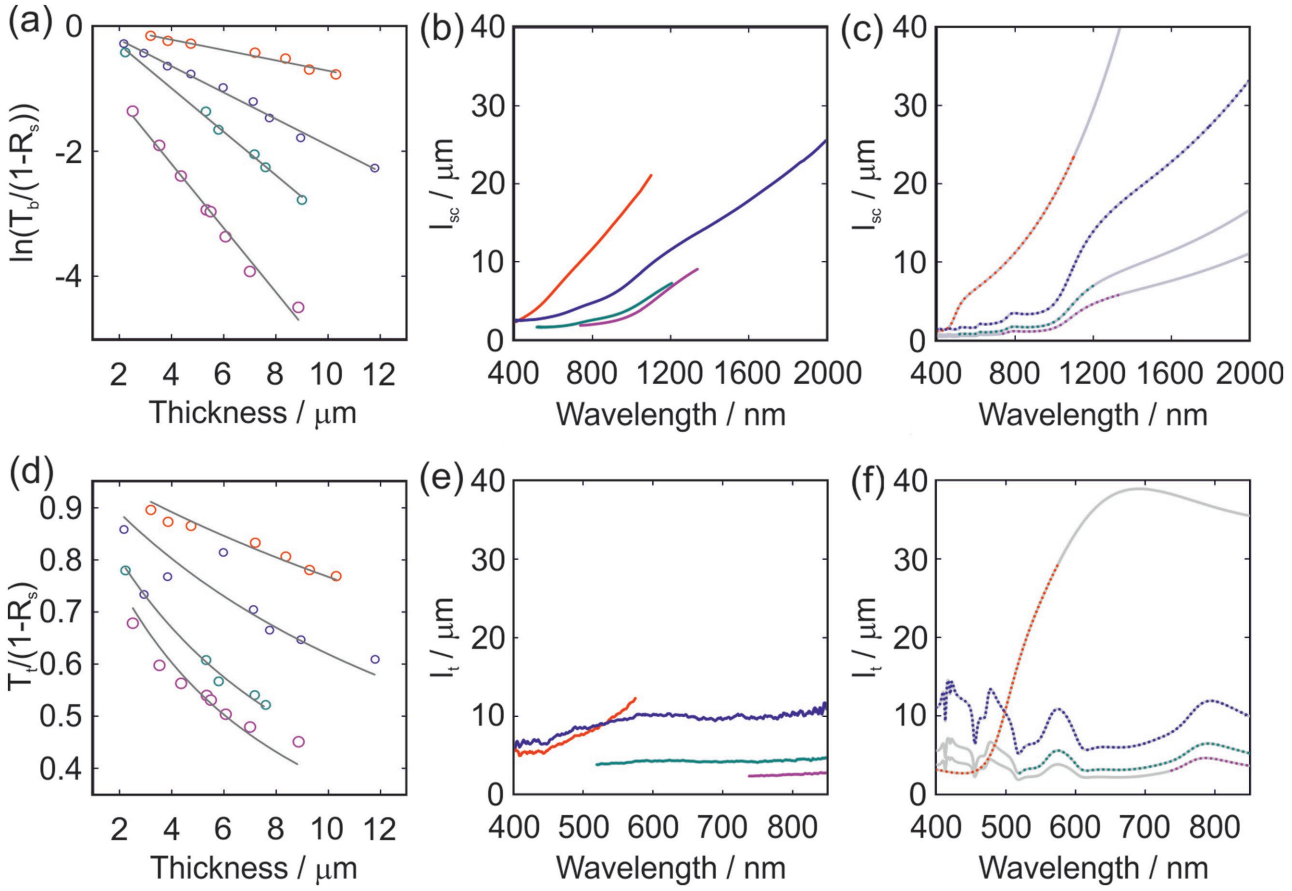

Figure 3. a) $\ln(T_b/(1-R_s))$ obtained from experimental measurements of ballistic transmittance (T_b) and specular reflectance (R_s) at $\lambda = 800$ nm as a function of film thickness for Mie glasses made of TiO_2 spheres of radius r embedded in a TiO_2 porous matrix at a filling fraction f, namely $r = 95 \pm 20$ nm and $f = 5\%$ (red symbols); $r = 225 \pm 20$ nm and $f = 5\%$ (blue symbols); $r = 225 \pm 20$ nm and $f = 10\%$ (green symbols), and $r = 225 \pm 20$ nm and $f = 15\%$ (magenta symbols). Gray lines represent linear fittings to the symbols according to Equation (4). b) Experimental and c) theoretical spectral dependence of the scattering mean free path of Mie glasses with $r = 95 \pm 20$ nm and $f = 5\%$ (red line); $r = 225 \pm 20$ nm and $f = 5\%$ (blue line); $r = 225 \pm 20$ nm and $f = 10\%$ (green line); and $r = 225 \pm 20$ nm and $f = 15\%$ (magenta line). d) $T_t/(1-R_s)$ obtained from experimental measurements of total transmittance (T_t) and R_s at $\lambda = 800$ nm as a function of film thickness for the Mie glasses discussed in (a)–(c). Gray curves represent fittings to the symbols according to Equation (5). e) Experimental and f) theoretical spectral dependence of the transport mean free path of the abovementioned Mie glasses.

to be significantly longer than the thickness of the fabricated films, thus preventing the reliable estimation of its magnitude. Also, as the particle concentration becomes higher, the correlation terms between scattering centers start to be significant at shorter wavelengths, thus limiting the validity of the model herein proposed. In order to gain insight into the angular distribution of the scattering in these media,[29] we study l_t. The propagation of light through a random medium is considered diffusive when the scattering strength is weak ($kl_{sc} \gg 1$). Such approximation is valid for distances greater than the average distance at which the direction of light is randomized by said scattering ($L \gg l_t$).[30] The diffusive regime is thus formulated through $\lambda \ll l_t \ll L$ and the spectral dependence of l_t can be determined from the fitting of the stationary solution of the diffusion equation[31]

$$\frac{T_t}{1-R_s} = \frac{1}{\alpha z_e} \frac{\sinh\left[\alpha(z_e + z_p)\right] \sinh\left[\alpha z_e\right]}{\sinh\left[\alpha(L + 2z_e)\right]} \tag{5}$$

where T_t is the total transmittance of the random medium, α is the extinction coefficient, and z_e and z_p are extrapolation and penetration lengths, respectively. The latter are usually considered to be equal and can be calculated according to[19,20]

$$z_p = z_e = \frac{1}{2\alpha} \ln\left(\frac{1+\alpha z_0}{1-\alpha z_0}\right) \tag{6}$$

and

$$z_0 = \frac{2}{3} l_t \left(\frac{1+R}{1-R}\right) \tag{7}$$

with R being the polarization-averaged Fresnel reflectivity at the interface between the disordered material and the embedding medium.[32] In particular, our random medium made of TiO_2 spheres dispersed in a mesoporous TiO_2 matrix yields $R = 0.07$ for $f = 5\%$, $R = 0.16$ for $f = 10\%$, and $R = 0.27$ for $f = 15\%$. Figure 3d shows the thickness dependence of $\frac{T_t}{1-R_s}$

at λ = 800 nm for the Mie glasses under analysis fitted to Equation (5) to extract l_t at this particular wavelength. Figure 3e displays the experimental l_t spectra. For r = 95 ± 20 nm and f = 5%, Equation (5) yields values of l_t longer than the thickest glass considered (~12 μm) for λ > 575 nm, being therefore not fulfilled the condition $l_t \ll L$. Hence, light propagation cannot be considered diffusive, Equation (5) is unable to describe the transport of photons for λ > 575 nm, and, consequently, values of l_t attained in this spectral range are not shown in Figure 3e. It can be observed that larger scattering centers or higher loading fractions lead to shorter values of l_t, being $l_t > l_{sc}$ for each wavelength as expected from scattering centers that yield nonisotropic scattering. Figure 3f shows the spectral dependence of l_t obtained from Equation (3). Good agreement is found between measured and calculated l_t, despite some discrepancies mainly observed for the glasses that present least scattering strength. It is also worth mentioning that the polydispersity of the scattering centers can also induce deviations in the behavior of the samples with respect to Mie predictions. As particles of diverse sizes sustain resonances for different wavelengths, collective excitations are smoothed out when the size distribution is not sharp enough. In addition, our model does not account for the fact that each TiO_2 sphere does not share the same geometrical center with its surrounding air shell. Disagreement between measured and calculated values is larger for the case of the transport mean free path, l_t, as it depends both on l_{sc}, which is a function of the scattering cross-section, and the angular distribution of scattered light, which is presumably more sensitive to the deviations of the scatterer shape from a perfect sphere. Despite such discrepancies, these results further confirm that our inhomogeneous solids behave as solid dispersions of spheres, being possible to describe also the angular scattering properties of our random media using Mie theory.

4.2. Mie Glasses for Color Conversion

As mentioned before, the porosity of the matrix allows the infiltration of chromophores, fluorophores, or polymers that bestows different functionalities on the system. So, finally, we perform an analysis of the spontaneous emission of Mie glasses and a reference, made exclusively of mesoporous TiO_2, after sensitizing them with a red fluorescent dye. This fluorophore shows chemical stability and high quantum yield, which makes it of interest for color conversion in solid-state lighting.[33] Excitation and fluorescence spectra of this dye are available in the Supporting Information. We measure the angular dependence of the emission by means of Fourier image spectroscopy; please see the Experimental Section for further details. The data shown in **Figure 4**a, corresponding to the reference layer, reveal a Lambertian distribution of the light emission as expected for an optically flat emitting layer. When TiO_2 scattering centers are integrated in the film the emission intensity is significantly enhanced while the angular profile is preserved, as it can be observed in Figure 4b. Indeed, a Lambertian profile of the emission is found regardless the size and concentration of the spheres as it is well illustrated in the Supporting Information.

We also characterized the emission of the Mie glasses and the reference in an integrating sphere, where light emitted in all possible directions is collected. Fluorescence spectra of Mie glasses with inclusions of r = 95 nm and f = 5%; r = 225 nm and f = 5%; and r = 225 nm and f = 10% (colored lines) are plotted in Figure 4c along with that for a reference film (black line) at the pumping wavelength λ_{pump} = 530 nm. The emission is enhanced for all Mie glasses, being possible to quantify the enhancement factor (η_{PL}) according to

$$\eta_{PL}(\lambda) = \frac{\int_{\lambda_1}^{\lambda_2} PL(\lambda)\,d\lambda}{\int_{\lambda_1}^{\lambda_2} PL_{ref}(\lambda)\,d\lambda} = \eta_{pump} \cdot \eta_{emi} \quad (8)$$

where PL(λ) is the photoluminescence spectrum of the Mie glass and $PL_{ref}(\lambda)$ is that of a layer of similar thickness devoid of scattering centers. The spectral dependence of η_{PL}, which, as expected, follows the trend imposed by the l_{sc} and l_t spectra, is shown in the Supporting Information. The emission enhancement depends on phenomena occurring both at the pumping (η_{pump}) and at the emission wavelength (η_{emi}) of the light-emitting molecules. Indeed, on the one hand, the emission intensity can be enhanced due to a resonant excitation, which causes the pumping light to be more efficiently absorbed by the dye molecules. As the scattering mean free path shortens, the probability of incident photons undergoing scattering events becomes larger and so does the average length of the path traveled by them through the film. This gives rise to longer matter–radiation interaction times, which results in increased absorption of the targeted wavelengths, in our case the excitation wavelength employed (λ_{pump} = 530 nm). On the other, the amount of emitted light can be enhanced due to (i) an enhanced outcoupling efficiency in defined directions and (ii) the spatial fluctuations of the local density of optical states (LDOS) that are expected in complex disordered media,[34,35] which may result in an improvement of the quantum yield of the system. However, only the former of these two effects should play a significant role in our Mie glass provided the low scattering strength that our materials feature. In turn, the outcoupling efficiency is expected to be enhanced due to the presence of the scattering centers, which are able to scatter light out of the material at angles above the escape cone, thus reducing light guiding along the layer. On the other hand, the photoemission intensity of the dye molecules embedded in the porous matrix will in principle depend on the radiative decay rate of the excited electron states, which in turn depends on the LDOS. No significant variation of the LDOS is expected as a result of the dilute dispersion of large scatterers present in the films. So, we may reasonably assume that no increase of the radiative decay rate of excited electrons and hence the quantum yield will be due to this effect. Improvement of the photoemission efficiency through the LDOS would entail the design of a very specific optical environment conceived to that purpose, which is not the case.

Figure 4d displays a bar plot of η_{PL} for the different Mie glasses considered at three different λ_{pump}, namely, λ_{pump} = 440 nm, λ_{pump} = 530 nm, and λ_{pump} = 575 nm. The size of each bar accounts for η_{PL}, corresponding the stripped region to η_{pump}, which equals the absorptance enhancement. Measurements of the absorptance of the different Mie glasses and

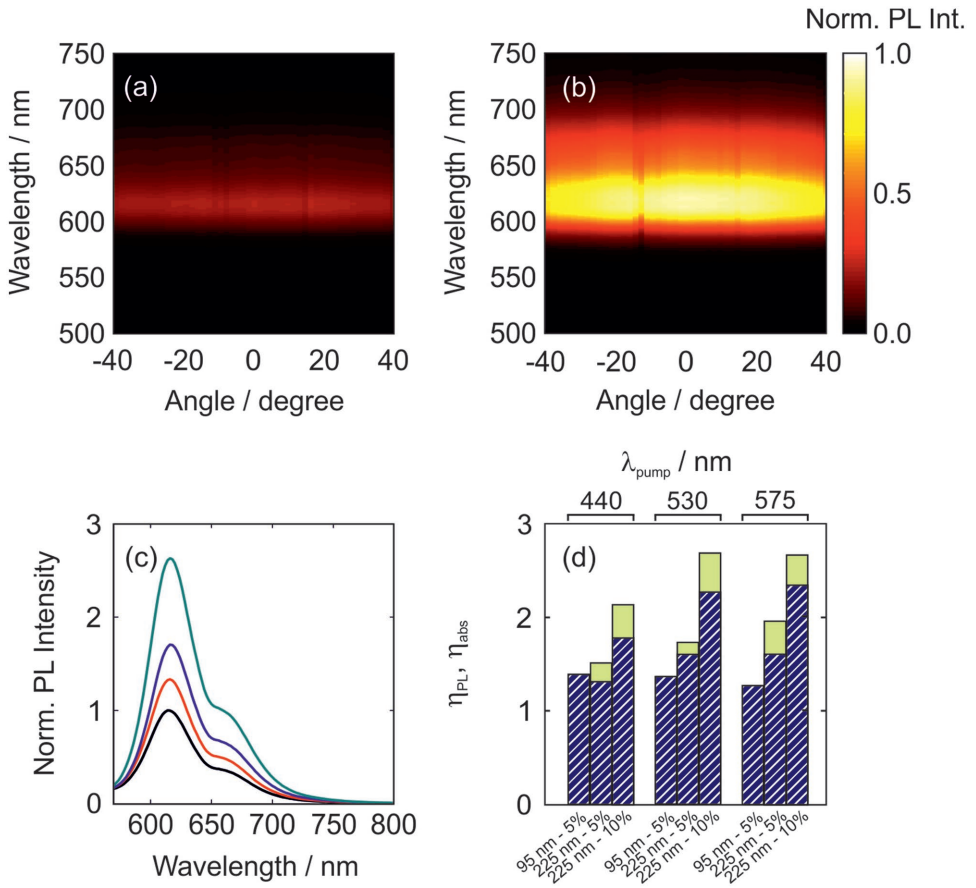

Figure 4. a,b) Fluorescence intensity as a function of the emitted wavelength and the angle of emission for a 7.5 µm thick mesoporous TiO_2 film sensitized with light-emitting dye molecules (a) and for a similar film containing scattering centers with $r = 225 \pm 20$ nm and $f = 10\%$ (b). c) Angular integrated fluorescence spectra measured from films incorporating spherical scatterers with $r = 95 \pm 20$ nm and $f = 5\%$ (red line); $r = 225 \pm 20$ nm and $f = 5\%$ (blue line); and $r = 225 \pm 20$ nm and $f = 10\%$ (green line). Each spectrum is normalized to the emission of reference layer of similar thickness without any light scatterers (black line). d) Representation of the fraction of the fluorescence enhancement integrated for all angles and wavelengths for the Mie glasses discussed in (c) at the three different pumping wavelengths: $\lambda_{pump} = 450$ nm, $\lambda_{pump} = 530$ nm, and $\lambda_{pump} = 575$ nm.

absorptance enhancement with respect to the reference layer are available in the Supporting Information. Results displayed in Figure 4d indicate that η_{PL} associated with the Mie glasses analyzed can be mainly attributed to an enhanced absorption caused by multiple scattering. An increase of either the size or the concentration of the inclusions yields a shorter l_{sc} and therefore a larger η_{pump} and thus η_{PL}. Hence the scatterer-loaded dyed film presents an effective absorption coefficient that is several times larger than the one it would show without particles embedded. We observe that η_{emi} of the different media is independent of λ_{pump}, showing higher η_{emi} for Mie glasses made of higher f due to the fact that they feature a shorter l_{sc}—see Figure 3c. We also observe that η_{PL} roughly equals η_{pump} for the Mie glass with $r = 95$ nm and $f = 5\%$ regardless of the pumping wavelength. Furthermore, although the difference is small, η_{pump} decreases for longer λ_{pump}, as l_{sc} dictates; see Figure 3c. We attain a maximum η_{PL} of 2.68 for the Mie glass with $r = 225$ nm and $f = 10\%$ when $\lambda_{pump} = 530$ nm, being $\eta_{pump} = 2.27$. Our results indicate that the fine control over the multiple scattering properties possible in Mie glasses provides a similar fine-tuning of the spontaneous emission intensity extracted over large areas.

5. Conclusion

We have developed a novel optically disordered material, which constitutes an example of a Mie glass, whose scattering properties can be defined prior to fabrication. It has been demonstrated that light propagation in our material can be described according to Mie theory based on the scattering properties of a single sphere, thus revealing that Mie glasses behave as solid suspension of spheres. Our method allows the realization of a deterministic design of the random medium in an unprecedented manner. In particular, it is possible to fix the scattering mean free path at will through a careful choice of the size and concentration of the dielectric scatterers included. Our Mie glass permits to enhance the spontaneous emission of light-emitting molecules. We measure a fluorescence enhancement close to three, which is attributed to a combination of resonant excitation and a better outcoupling of the emitted light. Mie glass is confirmed to be an inexpensive material to investigate fundamental aspects of light propagation through random media, showing great potential for applications in which a fine control over light absorption and improved light outcoupling are sought for. Future work will focus on the realization of such

inhomogeneous solids based on other materials that may offer higher dielectric constant contrast between scattering centers and matrix, hence opening the possibility to study different light transport regimes.

6. Experimental Section

Calculations: The scattering cross-section of the spheres required for the determination of the scattering mean free paths was semianalytically obtained through Mie formalism. As scattering centers, stratified spheres comprising two phases were considered, being the first phase an anatase sphere of radius r and the second a surrounding air layer with thickness $\approx 0.5r$. The scattering centers were embedded in an external medium, which consists of a mesoporous TiO_2 matrix, for which 50% porosity was assumed. Notice that, although the model allows consideration of the absorption of the materials through the complex refractive index, the materials comprising our simulated layers do not present absorption in the visible range. The complex refractive indices of the materials employed in the calculations are available in the Supporting Information.

Sample Preparation: The films were prepared from a paste containing a mixture of the small TiO_2 particles subsequently forming the mesoporous matrix and the submicron TiO_2 spheres serving as scattering centers. For the synthesis of the spheres the procedure reported by Kim et al. was followed,[36] which provides control over their size. The pastes were prepared according to a method described in detail elsewhere.[25] 3 mm thick glass slides were used as substrates for the deposition of the layers after a cleaning process of 15 min sonication in ethanol absolute. Layers of 1 cm^2 area and diverse thicknesses were deposited on the substrates via screen-printing from the previously prepared pastes. The thickness was varied by alternating screens with different meshes and changing the number of performed depositions. A process of evaporation of the solvent at 150 °C during 5 min was required in between deposition for stabilization of the film. Films with thicknesses ranging from ≈2 to ≈12 µm resulted after sintering.

As for the preparation of the emitting glasses, layers with thicknesses around 7 µm were immersed in a 0.075 wt% solution of a perylene dye (Lumogen F Red 305, BASF) in ethanol absolute during 24 h.

Structural Characterization: Cross-section pictures of the materials under study were obtained using a dual-beam Zeiss Auriga FIB-SEM. A beam of gallium ions was generated and focused in order to etch the film, followed by exploration of the resulting cross-section employing an accelerated electron beam.

The values of the thickness of the films for the determination of the l_{sc} curves were extracted and averaged from several cross-section SEM pictures of each film in different regions.

Optical Characterization: Measurements of the spectral ballistic transmittance and specular reflectance were performed using a UV–vis spectrophotometer (Cary 7000). Spectra were collected with an incident angle of 6° in the wavelength range comprised between 400 and 2000 nm.

The absorptance spectra of the sensitized films were collected employing an integrating sphere (Labsphere, 10 in.) coupled to an optical fiber guiding the light into a spectrophotometer (Ocean Optics, USB 2000+). To that aim, the layers were illuminated by white light (Ocean Optics, HL-2000) through different ports of the sphere, according to a standard procedure.

The angular dependence of the emission spectra was measured using a back focal plane microscope with which it is possible to attain the intensity distribution of the emitted light over all wave vectors in the numerical aperture (NA) of the objective. In particular, the films were excited with a 532 nm laser diode and their emission collected by a 100× objective with 0.75 NA. Each point of the back focal plane could be associated with one k-vector. Consequently, scanning an image of the back focal plane of the imaging objective using a fiber coupled spectrophotometer (Ocean Optics, USB 2000+) enabled attaining the emission spectrum as a function of the angle of the emission.

The angular integrated emission and excitation spectra of the sensitized films were collected using a double monochromator spectrofluorometer (Fluorolog-3 Horiba Jobin Yvon). The measurements were performed inside an integrating sphere in order to collect light emitted in all directions. The emission spectra were measured at three excitation wavelengths, λ_{pump} = 440, 530, and 575 nm, whereas the excitation spectra were measured at λ = 616 nm.

Supporting Information

Supporting Information is available from the Wiley Online Library or from the author.

Acknowledgements

Funding for the development of the research leading to these results was received from the European Research Council under the European Union's Seventh Framework Programme (FP7/2007–2013)/ERC grant agreement No. 307081 (POLIGHT) and the Spanish Ministry of Economy and Competitiveness under grant MAT2014-54852-R. The authors also thank the CITIUS for supporting them with the microstructural characterization. J.M.M. acknowledges the Spanish Ministry of Education, Culture and Sport for funding through an FPU program.

Keywords

color conversion, fluorescent materials, light diffusers, Mie scattering, TiO_2 nanoparticles

Received: January 10, 2017
Revised: February 7, 2017
Published online: April 6, 2017

[1] G. Mie, *Ann. Phys.* **1908**, *330*, 377.
[2] C. F. Bohren, D. R. Huffmann, *Absorption and Scattering of Light by Small Particles*, Wiley-Interscience, New York **2010**.
[3] Y. Kuga, A. Ishimaru, *J. Opt. Soc. Am. A* **1984**, *1*, 831.
[4] P. Wolf, G. Maret, *Phys. Rev. Lett.* **1985**, *55*, 2696.
[5] M. P. Van Albada, A. Lagendijk, *Phys. Lett. Rev.* **1985**, *55*, 2692.
[6] P. Wolf, G. Maret, E. Akkermans, R. Maynard, *J. Phys. (Paris)* **1988**, *49*, 63.
[7] M. B. van der Mark, M. P. van Albada, A. Lagendijk, *Phys. Rev. B* **1988**, *37*, 3575.
[8] S. Fraden, G. Maret, *Phys. Rev. Lett.* **1990**, *65*, 512.
[9] F. Scheffold, G. Maret, *Phys. Rev. Lett.* **1998**, *81*, 5800.
[10] N. M. Lawandy, R. M. Balachandran, A. S. L. Gomes, E. Sauvain, *Nature* **1994**, *368*, 436.
[11] A. Usami, *Chem. Phys. Lett.* **1997**, *227*, 105.
[12] Z. Wang, H. Kawauchi, T. Kashima, H. Arakawa, *Coord. Chem. Rev.* **2004**, *248*, 1381.
[13] S. Hore, P. Nitz, C. Vetter, C. Prahl, M. Niggemann, R. Kern, *Chem. Commun.* **2005**, *15*, 2011.
[14] E. Gross, N. Künzner, J. Diener, M. Fujii, V. Y. Timoshenko, D. Kovalev, *Phys. Status Solidi C* **2005**, *9*, 3268.
[15] V. P. Yashchuk, O. Prygodiuk, V. Koreniuk, E. Tikhonov, V. Bezrodny, *Appl. Phys. B* **2008**, *92*, 593.
[16] H. Cao, Y. G. Zhao, *Phys. Rev. Lett.* **1999**, *82*, 2278.

[17] C. Sommer, J. R. Krenn, *IEEE J. Sel. Top. Quantum Electron.* **2009**, *15*, 1181.
[18] W. L. Vos, T. W. Tukker, A. P. Mosk, A. Lagendijk, W. L. IJzerman, *Appl. Opt.* **2013**, *52*, 2602.
[19] M. Störzer, C. M. Aegerter, G. Maret, *Phys. Rev. E* **2006**, *73*, 065602(R).
[20] R. Sapienza, P. D. García, J. Bertolotti, M. D. Martín, A. Blanco, L. Viña, C. López, D. S. Wiersma, *Phys. Rev. Lett.* **2007**, *99*, 233902.
[21] P. D. García, R. Sapienza, J. Bertolotti, M. D. Martín, A. Blanco, A. Altube, L. Viña, D. S. Wiersma, C. López, *Phys. Rev. A* **2008**, *78*, 023823.
[22] P. D. García, R. Sapienza, C. López, *Adv. Mater.* **2010**, *22*, 12.
[23] V. Y. F. Leung, A. Lagendijk, T. W. Tukker, A. P. Mosk, W. L. IJzerman, W. L. Vos, *Opt. Express* **2014**, *22*, 8190.
[24] P. D. Kaplan, A. D. Dinsmore, A. G. Yodh, D. J. Pine, *Phys. Rev. E* **1994**, *50*, 4827.
[25] J. M. Miranda-Muñoz, S. Carretero-Palacios, A. Jiménez-Solano, Y. Li, G. Lozano, H. Míguez, *J. Mater. Chem. A* **2016**, *4*, 1953.
[26] M. Störzer, C. M. Aegerter, G. Maret, *Phys. Rev. E* **2006**, *73*, 065602(R).
[27] O. L. Muskens, S. L. Diedenhofen, B. C. Kass, R. E. Algra, E. P. A. M. Bakkers, J. Gómez-Rivas, A. Lagendijk, *Nano Lett.* **2009**, *9*, 930.
[28] S. Fraden, G. Maret, *Phys. Rev. Lett.* **1990**, *65*, 512.
[29] M. U. Vera, D. J. Durian, *Phys. Rev. E* **1996**, *53*, 3215.
[30] M. C. W. van Rossum, Th. M. Nieuwenhuizen, *Rev. Mod. Phys.* **1999**, *71*, 313.
[31] N. García, A. Z. Genack, A. A. Lisyanski, *Phys. Rev. B* **1992**, *46*, 14475.
[32] J. X. Zhu, D. J. Pine, D. A. Weitz, *Phys. Rev. A* **1991**, *44*, 3948.
[33] G. Lozano, D. J. Louwers, S. R. K. Rodriguez, S. Murai, O. T. A. Jansen, M. A. Verschuuren, J. G. Rivas, *Light: Sci. Appl.* **2013**, *2*, e66.
[34] M. D. Birowosuto, S. E. Skipetrov, W. L. Vos, A. P. Mosk, *Phys. Rev. Lett.* **2010**, *105*, 013904.
[35] R. Sapienza, P. Bondareff, R. Pierrat, B. Habert, R. Carminati, N. F. van Hulst, *Phys. Rev. Lett.* **2011**, *106*, 163902.
[36] Y. J. Kim, M. H. Lee, H. J. Kim, G. Lim, Y. S. Choi, N. Park, K. Kim, W. I. Lee, *Adv. Mater.* **2009**, *21*, 1.

